Pioneer Design of Non-contact Synchronized Measurement Devices Using Electric and Magnetic Field Sensors

Wenxuan Yao, *Student Member, IEEE,* Yingchen Zhang, *Senior Member, IEEE,* Yong Liu, *Member, IEEE,* Micah J. Till, *Student Member*, *IEEE,* Yilu Liu, *Fellow, IEEE,*

***Abstract*— Traditional synchrophasors rely on CTs and PTs physically connected to transmission lines or buses to acquire input signals for phasor measurement. However, it is challenging to install and maintain traditional phasor measurement units in some remote areas due to lack of facilities. Since transmission lines naturally generate alternating electrical and magnetic fields in the surrounding atmosphere, this paper presents two innovative designs for non-contact synchronized measurement devices (NCSMD), including an electric field sensor based non-contact SMD (E-NCSMD) and a magnetic field sensor based non-contact SMD (M-NCSMD). Compared with conventional synchrophasors, E-NCSMD and M-NCSMD are much more flexible to be deployed and have much lower costs, making E-NCSMDs and M-NCSMD highly accessible and useful for a wide array of phasor measurement applications. Laboratory and field experiment results verified the effectiveness of the designs of both E-NCSMD and M-NCSMD.**

***Index Terms*— Electric field, magnetic field, phasor measurement unit, non-contact synchronized measurement devices.**

I. Introduction

Synchrophasors greatly improve power grid observability using global positioning system (GPS) time-synchronized measurements [1]-[3]. Traditional synchrophasor, usually installed in substations at the transmission level, must be connected physically with a bus or line through potential transformers (PTs) and current transformers (CTs), which requires high manufacturing, installation, and maintenance costs [4][5]. For example, the installation cost of one transmission-level synchrophasor was more than $80,000 at the Tennessee Valley Authority (TVA) [6]. Such high cost obviously impedes large-scale deployment across the power grid.

Furthermore, in some remote areas, far from any substation, it is difficult to install and maintain a synchrophasor due to the lack of facilities. However, high voltage overhead transmission lines are indispensable components of the power grid and abnormal changes of parameters in any part of the transmission network may lead to serious damage or even interruption of power delivery [7]. Thus, there is a need to monitor the frequency and angle of overhead high voltage transmission lines in such areas to maintain reliable and stable operation across the entire grid. Therefore, portable and flexible phasor measurement devices are required.

Per electromagnetic theory, overhead transmission lines generate electric and magnetic fields simultaneously in their right-of-way corridors [8]-[9]. The magnetic fields of overhead power transmission lines are used for non-contact voltage monitoring in Ref. [10]. Since the frequency of these two fields reflects the frequency of the transmission line, it is, then, feasible to obtain frequency characteristic of the transmission line by sensing these two fields. An electric or magnetic sensor can be used to translate the alternating field signal into an alternating current or voltage signal. Thus, an input signal can be obtained without a direct connection. Based on this principle, this paper introduces two types of devices, one using each field type, an electric field sensor based non-contact synchronized measurement device (E-NCSMD) and a magnetic field sensor based non-contact synchronized measurement devices (M-NCSMD). Both E-NCSMD and M-NCSMD can perform frequency and angle measurement from ground-level of the overhead transmission line right-of-way corridor, which can work as supplementary of conventional synchrophasors for wide-area monitoring of the transmission network.

The rest of this paper is organized as follows: Section II provides the theoretical foundation of electric field and magnetic field signal acquisition. Section III presents the hardware structure and measurement algorithm for E-NCSMD and M-NCSMD. Section IV presents the laboratory and field experiment results of the proposed devices. Finally, the conclusions and future work are drawn in Section V.

II. Theoretical Foundation

In this section, the theoretical foundation for electric and magnetic field sensors are discussed, respectively.

A. Acquisition of Electric Field Signal

According to electromagnetic theory, a conductor produces an electric field in its surroundings [11]-[12]. The electric field in the vicinity of multi-conductor power lines can be evaluated by superimposing the contribution from each conductor [13]. For simplicity, consider three infinite and balanced transmission line with radius r, shown in Fig. 1, according to the Gauss's law [14], the combined electric field E of observed point P at the ground panel can be expressed as

This work made use of the Engineering Research Center Shared Facilities supported by the Engineering Research Center Program of the National Science Foundation and DOE under NSF Award Number EEC-1041877 and the CURENT Industry Partnership Program.

W. Yao, Y. Liu, M. Till and Y. Liu are with the Department of Electrical Engineering and Computer Science, the University of Tennessee, Knoxville, TN, 37996, USA (e-mails:wyao3@utk.edu, yliu66@utk.edu, mtill@utk.edu, liu@utk.edu)

Y. Zhang are with the National Renewable Energy Laboratory, Golden, CO 80401 USA (e-mail: Yingchen.Zhang@nrel.gov)

$$\boldsymbol{E} = \underbrace{\boldsymbol{p_a}\frac{\lambda_a}{2\pi\varepsilon_0 d_a}}_{\boldsymbol{E_a}} + \underbrace{\boldsymbol{p_b}\frac{\lambda_b}{2\pi\varepsilon_0 d_b}}_{\boldsymbol{E_b}} + \underbrace{\boldsymbol{p_c}\frac{\lambda_c}{2\pi\varepsilon_0 d_c}}_{\boldsymbol{E_c}} \quad (1)$$

where λ_a, λ_b, and λ_c are the electric charge density of the infinite lines, respectively. d_a, d_b and d_c are the perpendicular distance between the conductors and the observed point. ε_0 is the permittivity of free space. $\boldsymbol{p}_a$, $\boldsymbol{p}_b$, and $\boldsymbol{p}_c$ are the unit direction vectors for each transmission line which depends on the relative position between the conductors and the observed point.

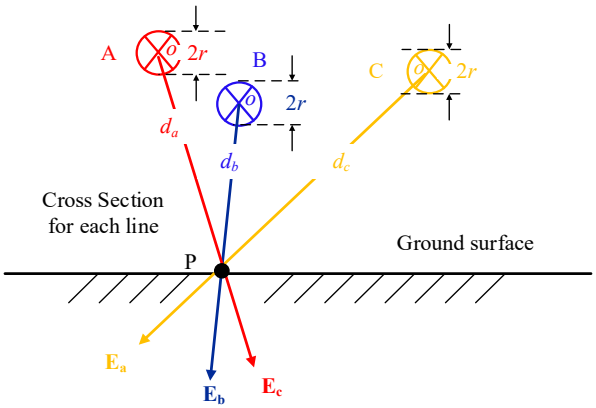

Fig. 1. Electric field calculation of three straight power line conductors.

For a balanced system, the voltage of the three transmission lines U_a, U_b and U_c are equal in frequency f, but displaced by 120° from one another, which can be expressed as

$$\begin{aligned} U_a &= |V_p|\cos(2\pi f t + \beta) \\ U_b &= |V_p|\cos(2\pi f t + \beta + 120°) \\ U_c &= |V_p|\cos(2\pi f t + 240°) \end{aligned} \quad (2)$$

where β is the initial angle.

The voltage for each transmission line can be calculated by integrating the electric field along the direction of the radius. Take line A as an example, according to the relationship between the voltage and electric field, the voltage can be expressed as

$$U_a = \int_r^{d_a} \frac{\lambda_a}{2\pi\varepsilon_0 r} dr = \frac{\lambda_a}{2\pi\varepsilon_0}\ln\left(\frac{d_a}{r}\right) \quad (3)$$

Substituting λ_a, λ_b, and λ_c into equation (1), the instantaneous strength of the electric field at point P can be expressed as

$$\boldsymbol{E} = \boldsymbol{p_a}\frac{U_a}{\ln\left(\frac{d_a}{r}\right)d_a} + \boldsymbol{p_b}\frac{U_b}{\ln\left(\frac{d_a}{r}\right)d_a} + \boldsymbol{p_c}\frac{U_c}{\ln\left(\frac{d}{r}\right)d_a} \quad (4)$$

Equation (4) indicates the frequency of the electric field at a fix point is equal to frequency of the conductor. The superposition principle can be applied to the angle and magnitude of the electric field vectors, which are determined by the relative position between the observed point and the transmission lines.

According to the IEEE 644-1994 standard [9], if the electric field is strong enough and is not overwhelmed by the environmental noise, it can be captured by a free-body meter as input signal for transmission line. Based on this idea, an electric field sensor is designed to replace traditional PTs and CTs for frequency and angle measurement. There are two parallel copper regions on the top layer and the bottom layer of printed circuit board to form a free-body meter. A small alternating electric potential will be induced between the two layers by the varying electric field, as shown in Fig. 2. Ideally, the dimension of the copper is infinite to avoid edge effect. Practically, to balance the tradeoff between the edge effect and portability, the dimensions of the electric sensor are determined as shown in Table I. This induced electric signal will be magnified by an amplifier circuit, formed with a voltage follower and an inverting negative feedback amplifier. To adapt the sensor for different electric field strengths, the gain ratios can be adjustable by changing the value of a variable resistor, as illustrated in Fig. 2. A low pass filter is used to block high frequency noise and isolate the low frequency component of the amplified signal V_{out1}. Then the filtered signal is fed into an ADC.

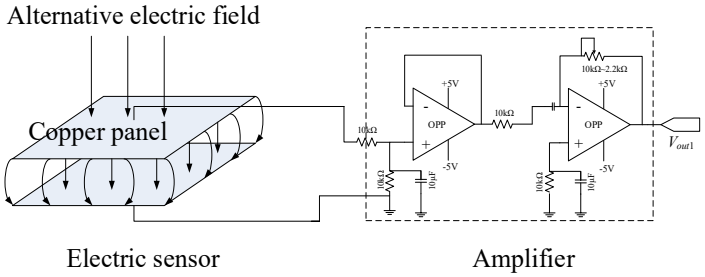

Fig. 2. Illustration of electric field sensor and amplifier circuit

TABLE I. DIMENSIONS OF ELECTRIC FIELD SENSOR

Length	Wide	Distance
5.05cm	3.05cm	0.16cm

B. *Acquisition of Magnetic Field Signal*

According to Ampere's Law, an AC current carrying conductor will produce a magnetic field in the surrounding atmosphere, as well as in nearby objects [15]. The magnetic field is perpendicular to the electric field. Based on the Biot–Savart Law, the emanated magnetic field from the currents in the phase conductors are correlated with the electrical parameters of the currents [16]-[18]. Therefore, it is possible to work inversely to find out the phasor information of the conductors by measuring and analyzing the emanated magnetic field. The strength of the magnetic field is proportional to the magnitude of current and is inversely proportional to the distance to the conductor. Consider the three infinite power current lines with AC current I_a, I_b, and I_c in Fig. 3. Based on Ampere's law [14], the magnetic field B at point Q can be expressed as

$$\boldsymbol{B} = \underbrace{\boldsymbol{q_a}\frac{I_a\mu}{2\pi l_a}}_{\boldsymbol{B_a}} + \underbrace{\boldsymbol{q_b}\frac{I_b\mu}{2\pi l_b}}_{\boldsymbol{B_b}} + \underbrace{\boldsymbol{q_c}\frac{I_c\mu}{2\pi l_c}}_{\boldsymbol{B_c}} \quad (5)$$

where μ is the magnetic permeability of the medium and $\boldsymbol{q_a}$, $\boldsymbol{q_b}$, and $\boldsymbol{q_c}$ are the unit direction vectors for each transmission line. l_a, l_b and l_c are the perpendicular distance between the conductors and the observed point. According to Faraday's Law, an electromotive force will be induced due to the changing of magnetic flux. For a balanced system, I_a, I_b and I_c have a frequency and magnitude at 120° angle separation as U_a, U_b,

and U_c in (2). Suppose there is an N-turns coil at the point Q, then the induced electromotive force, EF, can be expressed as

$$EF = N\frac{d\Phi}{dt} \tag{6}$$

where Φ is the total magnetic flux, which can be expressed as

$$\Phi = S \times (\cos\gamma_a \times B_a + \cos\gamma_b \times B_b + \cos\gamma_c \times B_c) \tag{7}$$

where S is the area of the coil and γ_a, γ_b, and γ_c are the angles between the magnetic field lines and perpendicular to the coil surface, respectively.

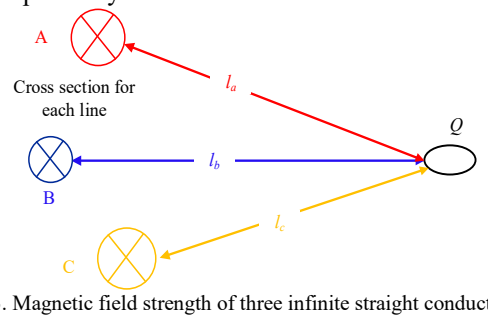

Fig. 3. Magnetic field strength of three infinite straight conductors.

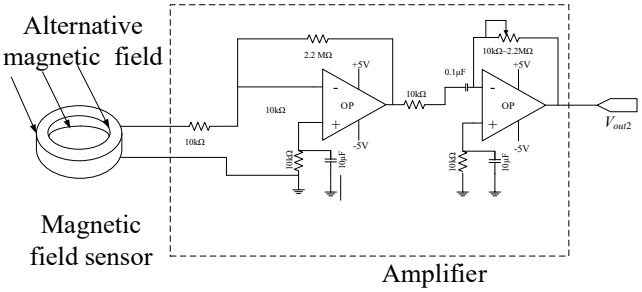

Fig. 4. Illustration of magnetic field sensor and amplifier circuit

According to (6) and (7), the strength of the induced voltage signal, EF is proportional to the size of the coil and the number of turns. Requiring a compromise between signal strength and the portability of the non-contact measurement device, the dimensions of the magnetic field sensor are given in Table II. Similar to the electric field sensor, a two stage amplifier circuit is used to amplify the induced voltage signal EF, as illustrated in Fig. 4. The gain ratio of the second stage is flexible to accommodate different signal strengths.

TABLE II. DIMENSIONS OF MAGNETIC FIELD SENSOR

Number of turns	Coil length	Coil diameter	
		Inner	External
1000	9cm	5cm	1cm

III. DEVICE PROTOTYPE DEVELOPMENT

The prototype development of E-NCSMD and M-NCSMD are discussed in this section. First, the hardware designs for these two types of non-contact SMD are introduced. Then, the single phase angle and frequency measurement algorithms adopted in E-NCSMD and M-NCSMD are presented.

A. Hardware Design

The E-NCSMD and M-NCSMD are both developed on the Frequency Disturbance Recorders (FDR) platform [19]-[22]. The non-contact sensors replace the potential transducer in FDRs for signal input. Besides the sensors, the E-NCSMD and M-NCSMD consist of a GPS receiver, a digital signal processor (DSP), microprocessor (MCU), data transceiver module, and solar battery module. The DSP is a TMS320LF2407 model, which is a 16 fix-point processor with the main core clock 30 MHz. The hardware design is shown in Fig. 5. The electric field sensor and magnetic field sensor are used to acquire input signals for the E-NCSMD and M-NCSMD, respectively. A low-pass filter with a cut-off frequency of 150 Hz rejects high-frequency noise and harmonic inference. By demodulating the GPS signal, GPS receivers can align their time with UTC time and output a high precision pulse per second (PPS) signal for time synchronization [23]. Since the error of PPS with a stable GPS signal is less than 30 nanoseconds [24], the rising edge of the PPS is used to trigger an interrupt in the DSP and consequently trigger the first sampling command to the ADC each second, as illustrated in Fig. 6. The length of each synchronous sampling cycle is 1 second to match the PPS. From the second sample to last sample between adjacent PPS signals, the sampling interval is controlled by a timer in the DSP through the serial peripheral interface (SPI) bus. The DSP also performs phasor estimation and then transmits the measurements to the MCU. The measurements are time-stamped in the MCU and sent out from the data transceiver. The total power consumption for both the E-NCSMD and M-NCSMD are less than 5 watts each, which can be provided by the solar battery module.

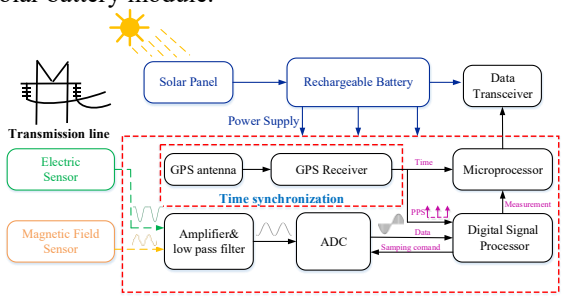

Fig. 5. Hardware design of the E-NCSMD and M-NCSMD

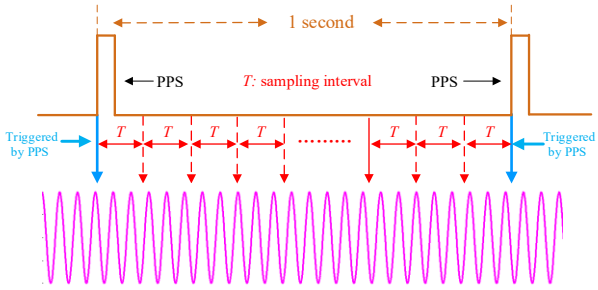

Fig. 6. Illustration of synchronous sampling for phasor measurement

B. Angle Monitoring Algorithm

A reliable algorithm is a crucial for the non-contact SMD. Unlike traditional SMDs which use three-phase inputs, the proposed non-contact devices only use a combined single-phase signal for phasor measurement. Thus, a single-phase recursive discrete Fourier transform (RDFT) is developed for angle monitoring. To reduce the fixed offset and sinusoidal oscillation in angle error for the single-phase DFT, the full three-phase signals and their symmetrical components are simulated from the single-phase signal under the assumption of a balanced

system [25]. Thus, RDFT is performed for the positive sequence of the simulated three phase signal. Given N data points of signal $\{x_k\}$ per cycle $k \in [1\ N]$, the phasor of the fundamental frequency components is

$$\bar{X}_{(1)} = \frac{1}{\sqrt{2}}\left(X^c_{(1)} + jX^s_{(1)}\right) \tag{8}$$

where

$$X^c_{(1)} = \frac{2}{N}\sum_{k=1}^{N} x_k \cos\left(\frac{2\pi k}{N}\right) \tag{9}$$

$$X^s_{(1)} = \frac{2}{N}\sum_{k=1}^{N} x_k \sin\left(\frac{2\pi k}{N}\right) \tag{10}$$

After the one cycle DFT initialization for $\bar{X}_{(1)}$, the successive $\bar{X}_k$ phasor for incoming data x_{k+N} can be recursively computed from $\bar{X}_{(k-1)}$ and the data points x_k and x_{k+N} satisfying

$$\bar{X}_{(k)} = \bar{X}_{(k-1)} + j\frac{\sqrt{2}}{N}(x_{N+k} - x_k)e^{-\left(j\frac{2\pi}{N}(k-1)\right)} \tag{11}$$

The angle of the k-th phasor is given by

$$\boldsymbol{\theta}_k = \tan^{-1}\left(\frac{X^c_{(k)}}{X^s_{(k)}}\right) \tag{12}$$

C. Frequency Monitoring Algorithm

Since the frequency is defined as the derivation of angle, frequency can be measured by calculating the rate of change of the angle. The first calculated frequency can be obtained by

$$f_1 = f_0 + \Delta f_{(1)} \tag{13}$$

where f_0 is nominal frequency (e.g., 60 Hz) and $\Delta f_{(1)}$ is the first frequency delta calculated from the rate of change of the angle through a least-square approximation [26], assuming the angle varies as a polynomial function with respect to the sampling number. Simulation results [27] show that the linear function cannot provide enough accuracy while the cubic function (and higher orders) does not improve accuracy significantly over the quadratic function, but carries higher computational overload. Therefore, the quadratic function is used for polynomial fitting as

$$\theta_{(m)} = \alpha_0 + \alpha_1 m + \alpha_2 m^2 \tag{14}$$

where m is index for the angle. α_0,α_1 and α_2 are the coefficient for quadratic function. Converting equation (14) into matrix form, it can be expressed as

$$\boldsymbol{\theta} = \boldsymbol{\alpha M} \tag{15}$$

Where angle matrix $\boldsymbol{\theta} = [\theta_{(1)} \cdots \theta_{(v)} \cdots \theta_{(V)}]$, coefficient matrix $\boldsymbol{\alpha} = [\alpha_0, \alpha_1, \alpha_2]$ and $\boldsymbol{M}$ is a constant valued matrix satisfying

$$\boldsymbol{M} = \begin{bmatrix} 1 & 1 & 1 \\ \vdots & \vdots & \vdots \\ 1 & M & M^2 \end{bmatrix} \tag{16}$$

where M is number of angle used for frequency calculation.

As the matrices $\boldsymbol{M}$ and $\boldsymbol{\theta}$ are known, the coefficient $\boldsymbol{\alpha}$ can be obtained by pseudo-inverse computation as

$$\boldsymbol{\alpha} = [\boldsymbol{M^T M}]^{-1}\boldsymbol{M^T \theta} \tag{17}$$

Therefore, the first frequency delta can be obtained as

$$\Delta f_{(1)} = \frac{1}{2\pi} N f_0(\alpha_1 + 2\alpha_2 m) \tag{18}$$

To further improve accuracy, f_1 will be regarded as the nominal frequency of the re-sampling process. The input signal is resampled via mathematical interpolation by maintaining a constant number of data points per sampling cycle. It is expected that the closer nominal frequency and actual frequency are, the more accurate the frequency estimation result will be. The i^{th} calculated frequency is

$$f_i = f_{i-1} + \Delta f_{(i)} \tag{19}$$

where Δf_i is the i^{th} frequency delta and f_{i-1} is the $(i\text{-}1)^{\text{th}}$ calculated frequency. Generally speaking, increasing the stages of resampling process helps improve the frequency estimation accuracy, but also incurs higher computational burden. Detail analysis in Ref.[27] reveal that a two-stage frequency estimation algorithm can sufficiently satisfy the requirement of power system frequency measurement.

IV. Performance Evaluation

The aim of this section is to validate the accuracy and effectiveness of E-NCSMD and M-NCSMD in terms of angle and frequency measurement accuracy by means of laboratory and field tests. A comparison between proposed non-contact SMDs and FDRs are also conducted.

A. Laboratory Experiment

It is generally accepted that electric and magnetic field strength in the right-of-way of 500kV transmission corridors is approximately in the range of 1 μT to 3 μT and 0.3 kV/m to 10 kV/m, respectively[28][29]. Therefore, in this laboratory experiment, to simulate the condition at the edge of a power line right-of-way, a 2 μT magnetic field and 5 kV/m electric field are generated via the magnetic source coil and electric source plate, respectively. The length and width of the source plates are 30.48 cm and 15.25 cm, respectively. The distance between the two source plates is 2.4 cm.

The Doble F6150 power system simulator with GPS signal synchronization is used to generate AC power for the source plate and source coil. The system setting is shown in Fig. 7. The experiment results of both kinds of NCSMDs are compared with an FDR, which can achieve frequency and angle accuracy of 0.5 mHz and 0.02° [30][31].

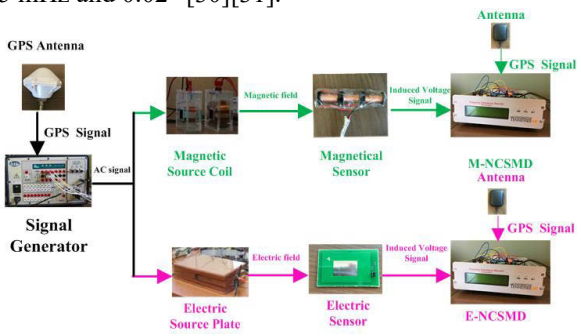

Fig. 7. Laboratory experiment setup

The angle and frequency measurement results over an ideal sinusoidal 60 Hz signal from the Doble signal generator are shown in Fig. 8 and Fig. 9. According IEEE standard C37.118.1, the limits for frequency and angle measurement on the stead-state condition are 0.005 Hz and 0.57° respectively

[32]. The maximum errors of frequency and measurements are listed in Table III. From Fig. 8 and Table III, the angle error for the E-NCSMD and M-NCSMD are within 0.04° and 0.07° while that of the FDR is 0.03°. The frequency measurement error of the E-NCSMD and M-NCSMD are within 1.82E-3 Hz and 2.51 E-3, respectively, while that of the FDR is 0.78 E-3 Hz, as seen listed in Table III.

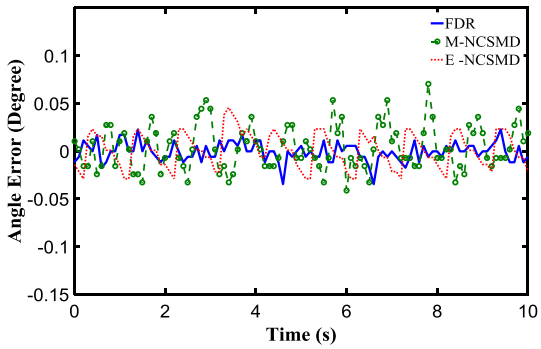

Fig. 8. Angle measurement results

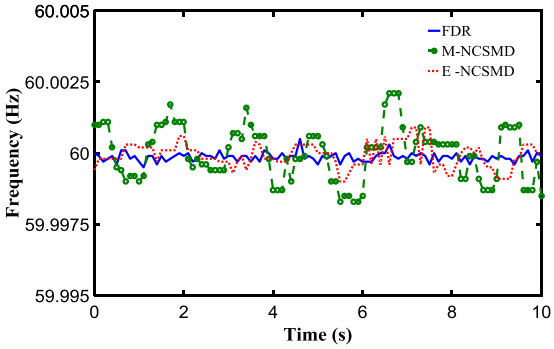

Fig. 9. Frequency measurement results

TABLE III. MAXIMUM ERROR FOR FREQUENCY (HZ) AND ANGLE (°)

Maximum Error	FDR	E-NCSMD	M-NCSMD
Frequency	5.78E-4	1.82E-3	2.51E-3
Angle	2.88E-2	3.56E-2	7.25E-2

TABLE IV. STANDARD DEVIATION OF FREQUENCY ERROR (HZ)

Input signal Frequency(Hz)	FDR	E-NCSMD	M-NCSMD
59.90	3.25E-4	8.25E-4	1.82E-3
59.98	2.33E-4	9.33E-4	1.98E-3
60.00	1.89E-4	3.89E-4	5.98E-4
60.02	3.60E-4	9.60E-4	1.96E-3
60.10	5.28E-4	9.28E-4	1.92E-3

TABLE V. STANDARD DEVIATION OF ANGLE ERROR(°)

Input signal Frequency(Hz)	FDR	E-NCSMD	M-NCSMD
59.90	1.75E-2	1.88E-2	3.41E-2
59.98	1.54E-2	1.76E-2	2.87E-2
60.00	9.51E-3	2.58E-2	3.25E-2
60.02	1.81E-2	2.57E-2	3.61E-2
60.10	1.91E-2	2.61E-2	3.65E-2

By varying the output frequency of the signal generator, the performance of the E-NCSMD and M-NCSMD can be evaluated under different conditions. The standard deviation (STD) is used to evaluate the frequency and angle error under fixed-frequency conditions. The comparison of frequency and angle results are listed in Table IV and Table V. The standard deviation of the frequency measurement result for the E-NCSMD and M-NCSMD is within 9.60 E-4 Hz and 1.96 E-3 Hz, compared to 5.28E-4 Hz for the FDR. For the angle measurement, the STD for the E-NCSMD and M-NCSMD are within 2.61 E-2° and 3.65 E-2°, compared with 1.91 E-2° for the FDR. The results demonstrate that the E-NCSMD and M-NCSMD are able to achieve almost the same accuracy in frequency and angle measurement as the FDR under steady-state conditions. The total vector error of E-NCSMD and M-NCSMD, as small as about 0.03% and 0.04% respectively, sufficiently complies with IEEE standard C37.118.1, which requires that TVE should be less than 1% [32].

B. Field Experiment

To further the accuracy and effectiveness of frequency and angle monitoring of non-contact SMDs in a field environment, the E-NCSMD and M-NCSMD are tested under 500 kV transmission line in Knoxville, Tennessee. An FDR installed in the same city at distribution level acts as reference for the comparison. Fig. 10 shows the setup of this field experiment. All the devices are required to sustain stable GPS signals for time synchronization throughout the test so the measurement results can be compared via identical GPS based timestamp. The computers in Fig. 10 is installed with FNET/Grideye sever client to receive the measurement data from NCSMD via TCP/IP.

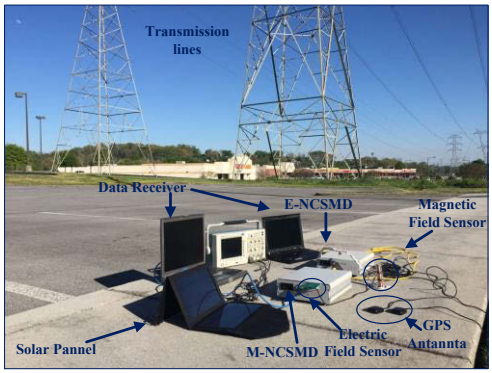

Fig. 10. Field experiment setup

The waveforms captured by different sensors are illustrated in Fig. 11. There is an obvious of phase difference between the signal captured by the electric field sensor and magnetic sensor. This is mainly due to the involvement of both inductive and capacitive components in amplifier and analog filters with different time constants, possible phase lag or advance may be introduced. However, this initial angle difference can be considered as constant and thus can be cancelled out. Furthermore, compared with conventional PT, obvious distortion of the signal from the non-contact sensors can be seen. Applying Fast Fourier Transform (FFT) to the signals in Fig. 11 yields the results of harmonic components analysis shown in Fig. 12. For the electric sensor, the dominant harmonics components are the 2nd, 3rd, and 4th order. For the magnetic

sensor, the 3rd, 5th, and 8th harmonics are the major components. Ref. [25]-[27] provide simulation experiments for frequency and angle accuracy under harmonic distortion using RDFT with different window length. The simulation results show that the error for frequency and angle measurements under 10% THD harmonic components within 1.23E-3 Hz and 7.21E-2° using a six-cycle RDFT. Since a six-cycle RDFT can achieve satisfactory accuracy under harmonic distortion, it is used in NCSMDs for frequency and angle calculation. Furthermore, there is also DC offset in the signal from the electric field sensor, causing clipping of the signal. The DC offset can be removed since the serial capacitor in the low pass filter can block DC component in the signal. The DC offset for the waveform is reduced from 0.13 to 0.04 p.u.

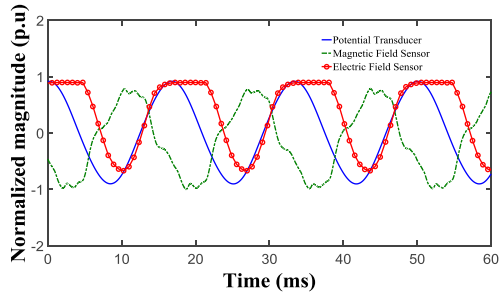

Fig. 11. Waveforms captured by three types of sensors

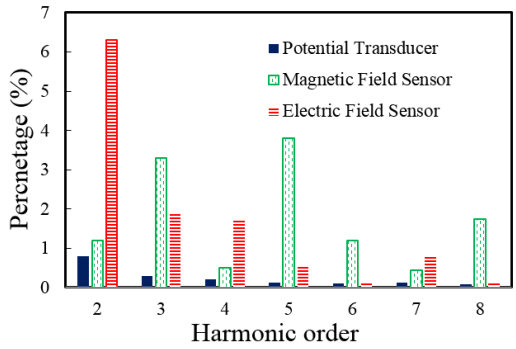

Fig. 12. Harmonic component analysis

Angle and frequency measurement results for a 250-second window are plotted in Fig. 13 and Fig. 14, respectively, at a reporting rate of 10 Hz. The E-NCSMD and M-NCSMD are able to achieve the same accuracy as the FDR except for some small spikes in the frequency result. After compensating by a constant value, phase difference between the FDR and NCSMD are within 0.5° as shown Fig. 13. The E-NCSMD and M-NCSMD are both able to efficiently capture the trends of frequency and angle change over time. The correlation coefficient of the frequency result between the E-NCSMD and M-NCSMD to the FDR are 0.9760 and 0.9736, respectively. After calibrating the constant time delay, the angle measurement errors are within 0.1° for both the E-NCSMD and M-NCSMD. The non-contact devices and FDR's measurement data have similar distributions in terms of angle and frequency, as shown in Fig. 15 and Fig. 16, which demonstrates that frequency and angle measurements of the non-contact devices fall into the same accuracy category as the FDR measurements. The error of frequency and angle measurement of the non-contact SMDs can be obtained using the FDR results as a reference. The maximum and STD of frequency and angle error are listed in Table VI. The total vector error of E-NCSMD and M-NCSMD for power grid signal are 0.04% and 0.05% respectively, which sufficiently meets 1% requirement in IEEE synchrophasor standard C37.118.1 [32] and are even more accurate than some commercial phasor measurement units.

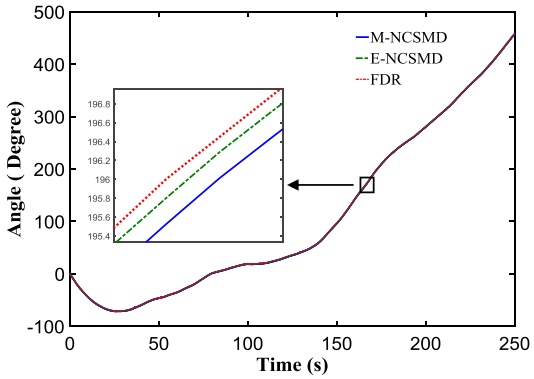

Fig. 13. Angle measurement results

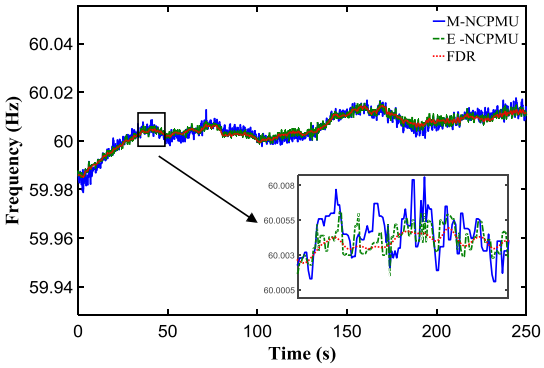

Fig. 14. Frequency measurement results

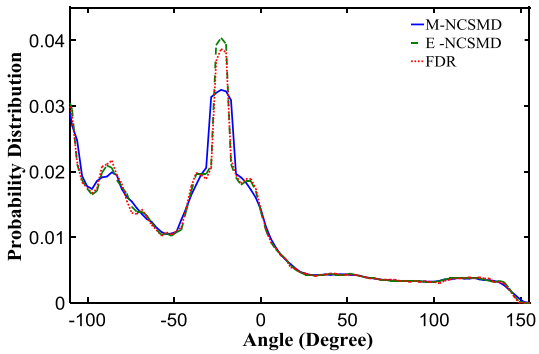

Fig. 15. Distribution of angle measurement

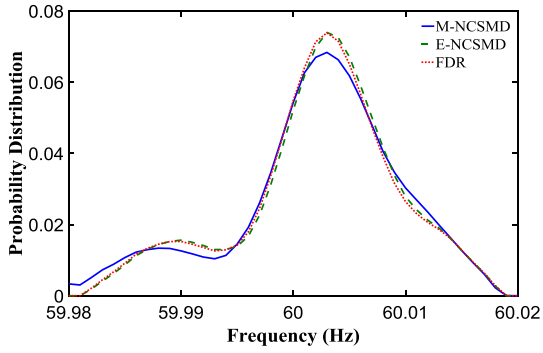

Fig. 16. Distribution of frequency measurement

TABLE VI. MEAUREMENT ERROR

Error	M-NCSMD		E-NCSMD	
	Max	STD	Max	STD
Frequency (Hz)	8.21E-3	7.55E-4	6.31E-3	1.78E-3
Angle (°)	9.78E-2	5.9E-2	8.00E-2	1.61E-2

To further verify the effectiveness of the non-contact measurement devices, the performance of developed devices are evaluated under a real power system event. Fig. 17 shows the frequency measurement obtained from M-NCSMD, E-NCSMD and an FDR for an 850MW generation trip event in the U.S. Eastern Interconnection. During this event, the real power grid frequency drops more than 50 mHz. From Fig. 17, M-NCSMD and E-NCSMD are capable of capturing the change of frequency in this event as accurately as the FDR.

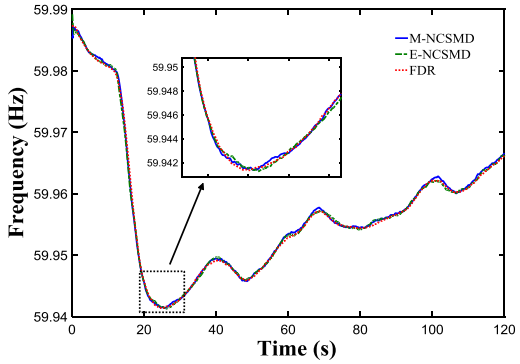

Fig. 17. Frequency measurement comparison of a generation trip event

The main challenge for these non-contact SMDs is to realize non-contact measurement with efficient, compact, and low cost field sensors without impairing the phasor measurement accuracy. Overall, the field test is successful and shows promising results, which demonstrates the non-contact frequency and angle measurement for overhead transmission line are feasible. The non-contact SMD has the advantage of portability, easy installation and low-cost compared with conventional synchrophasors. Nevertheless, at the current stage, the M-NCSMD and E-NCSMD have weakness in the robustness and are more sensitive to the environmental noise and interference compared with traditional CT/PT based synchrophasors. Therefore, to improve the robustness and reliability, a more effective filter is needed for noise reduction in the future for M-NCSMD and E-NCSMD.

V. CONCLUSION AND FUTURE WORK

In this paper, the design and implementation of two types of non-contact synchronized measurement devices, M-NCSMD and E-NCSMD, were presented. Laboratory and field experiments verified the effectiveness and accuracy of the angle and frequency measurements from both devices. Unlike traditional SMD, the proposed devices are portable and flexible, greatly broadening the synchrophasor family. Furthermore, these devices can reduce manufacturing and installation costs dramatically, facilitating wide application of future wide-area phasor monitoring of the transmission line network. Further work includes further improving the reliability and accuracy of both devices under noisy conditions via more advanced sensor integration, magnitude measurement realization, dynamic performance evaluation, waterproof design, wireless communication, lightning protection, and field tests in hostile weather and locations.

VI. REFERENCES

[1] A. G. Phadke and J. Thorp, Synchronized Phasor Measurements and Their Applications. New York, NY, USA: Springer, 2008.

[2] A. G. Phadke, “Synchronized phasor measurements in power systems,” IEEE Comput. Appl. Power, vol. 6, no. 2, pp. 10–15, Apr. 1993.

[3] J. Chai, J. Zhao, W. Yao, J. Guo and Y. Liu, "Application of Wide Area Power System Measurement for Digital Authentication", in Proc. *2016 IEEE T&D Conference and Exposition,* pp.1-5.

[4] Y. Zhang, W. Yao, J. Culliss, G. Zhang, Z. Teng and Y. Liu, "Electrical field based wireless devices for contactless power gird phasor measurement," in *Proc. 2014 IEEE PES General Meeting*, pp. 1-5.

[5] A. Mazloomzadeh, M. H. Cintuglu and O. A. Mohammed, "Development and evaluation of a laboratory based phasor measurement devices," Innovative Smart Grid Technologies Conference (ISGT), 2015 IEEE Power & Energy Society, Washington, DC, 2015, pp. 1-5.

[6] H. Lu, L. Zhan, Y. Liu and W. Gao, "A Microgrid Monitoring System Over Mobile Platforms," *IEEE Trans. Smart Grid* , vol.PP, no.99, pp.1-10

[7] X. Sun, Q. Huang, Y. Hou, L. Jiang and P. W. T. Pong, "Noncontact Operation-State Monitoring Technology Based on Magnetic-Field Sensing for Overhead High-Voltage Transmission Lines," *IEEE Trans. Power Delivery*, vol. 28, no. 4, pp. 2145-2153, Oct. 2013.

[8] “Transmission Line Reference Book, 345kV and Above/Second Edition”, EPRI, 1982.

[9] IEEE Standard Procedures for Measurement of Power Frequency Electric and Magnetic Fields from AC Power Lines, IEEE STD 664, 1994, Reaffirmed 2008

[10] K. Zhu, W. K. Lee and P. W. T. Pong, "Non-Contact Electric-Coupling-Based And Magnetic-Field-Sensing-Assisted Technique For Monitoring Voltage Of Overhead Power Transmission Lines," SENSORS, IEEE, Busan, 2015, pp. 1-4.

[11] Y. Liu, W Yao, L. Zhan, H. Lu and Wei Gao,"Mobile Electric Field Sensor Based Phasor Measurement Unit For Monitoring An Electric Power Grid", U.S. Patent. Application No. 20160025785, 2016

[12] G. Wijeweera, Bahreyni, Behraad, C. Shafai, A Rajapakse, D.R. Swatek, "Micromachined Electric-Field Sensor to Measure AC and DC Fields in Power Systems,", *IEEE Trans. Power Delivery*, vol.24, no.3, pp.988,995, July 2009

[13] R. Zeng; Y. Zhang; W. Chen and B. Zhang, "Measurement of electric field distribution along composite insulators by integrated optical electric field sensor,", *IEEE Trans. Dielectrics and Electrical Insulation*, vol.15, no.1, pp.302-310, February 2008

[14] G. S. N. Raju. Electromagnetic Field Theory and Transmission Lines, , India: Pearson, June, 2006

[15] P. Gao, S. Lin and W. Xu, "A Novel Current Sensor for Home Energy Use Monitoring," *IEEE Trans. Smart Grid, vol*. 5, no. 4, pp. 2021-2028, July 2014.

[16] X. Sun, Q. Huang, L. J. Jiang and P. W. T. Pong, "Overhead High-Voltage Transmission-Line Current Monitoring by Magnetoresistive Sensors and Current Source Reconstruction at Transmission Tower," *IEEE Trans. Magnetics*, vol. 50, no. 1, pp. 1-5, Jan. 2014.

[17] Q. Huang, W. Zhen and P. W. T. Pong, "A Novel Approach for Fault Location of Overhead Transmission Line With Noncontact Magnetic-Field Measurement," *IEEE Trans. Power Delivery*, vol. 27, no. 3, pp. 1186-1195, July 2012.

[18] G. Zhang, Y. Liu, Y. Zhang. "Accurate Magnetic Field Sensor And Method for Wireless Phasor Measurement Unit". U.S. Patent. Patent No. 8437969, 2010

[19] Y. Liu et al., "Wide-Area-Measurement System Development at the Distribution Level: An FNET/GridEye Example," IEEE Trans. Power Delivery, vol. 31, no. 2, pp. 721-731, April 2016.

[20] L. Zhan, Y. Liu, W. Yao, J. Zhao and Y. Liu, "Utilization of Chip Scale Atomic Clock for Synchrophasor Measurements," *IEEE Trans. Power Delivery*, vol.31, 5, Oct., 2016, pp.2299-2230

[21] S. You, J. Guo, W. Yao, S. Wang, Y. Liu, and Y. Liu, "Ring-down oscillation mode identification using multivariate empirical mode decomposition", in *Proc. 2016 IEEE Power and Energy Society General Meeting*, pp. 1-5.

[22] Y. Liu et al., "A Distribution Level Wide Area Monitoring System for the Electric Power Grid–FNET/GridEye," IEEE Access, vol. 5, no. , pp. 2329-2338, 2017.

[23] W. Yao, D. Zhou, L. Zhan, Y. Liu, Y. Cui, S.You, Y. Liu, "GPS signal loss in the wide area monitoring system: Prevalence, impact, and solution", Electric Power Systems Research, Vo.147,pp 254-262, June 2017

[24] W. Yao, et al , "Impact of GPS Signal Loss and Its Mitigation in Power System Synchronized Measurement Devices," *IEEE Trans. Smart Grid*, Early Access, 2016

[25] T. Xia and Y. Liu, "Single-Phase Phase Angle Measurements in Electric Power Systems," *IEEE Trans. Power Systems*, vol. 25, no. 2, pp. 844-852, May 2010.

[26] X. Zhang, "High precision dynamic power system frequency estimation algorithm based on phasor approach," Master. Dissertation, Virginia Plytechnic Institue and State University, Blacksburg, VA, 2004.

[27] J. Chen, "Accurate Frequency Estimation with Phasor Angles," Master. Dissertation, Electrical Engineering, Virginia Plytechnic Institue and State University, Blacksburg, VA, 1994.

[28] G.B. Iyyuni and S.A. Sebo, " Study of transmission line magnetic fields", Power Symposium, 1990. Proceedings of the Twenty-Second Annual North American 15-16 Oct. 1990.pp:222-231.

[29] F. Rahmatian, P.P Chavez, N. Jaeger, "230 kV optical voltage transducers using multiple electric field sensors,", *IEEE Trans. Power Delivery*, vol.17, no.2, pp.417-422, Apr 2002

[30] J. Chai, J. Zhao, W. Yao, J. Guo and Y. Liu, "Application of Wide Area Power System Measurement for Digital Authentication", in Proc. *2016 IEEE T&D Conference and Exposition,* pp.1-5.

[31] W. Yao, L. Zhan, Y. Liu, M. Till, J. Zhao, L. Wu, Z. Teng, Y. Liu, "A Novel Method for Phasor Measurement Unit Sampling Time Error Compensation," *IEEE Trans. Smart Grid*, Early Access, 2016.

[32] IEEE Standard for Synchrophasors for Power System, C37.118, IEEE Power System Relaying Committee of the Power Engineering Society, 2011.

BIOGRAPHY

Wenxuan Yao (S'14) received his B.S. degree in electrical engineering from Hunan University, Changsha, China, in 2011. He is pursuing the Ph.D. degree in the Department of Electrical Engineering and Computer Science, University of Tennessee, Knoxville.

His research interests include wide-area power system monioring, synchrophasor measurement applications, embeded system development, power quality diagnoisis and big data analysis for power system.

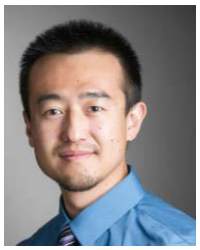

Yingchen Zhang (M'07-SM'16) received his B.S. degree from TianjinUniversity, China, in 2003 and his Ph.D. degree from Virginia Polytechnic Institute and State University in 2010. He is a senior engineer at the National Renewable Energy Laboratory, a visiting research assistant professor at the University of Denver, and an adjunct faculty member at Colorado State University.

His key areas of expertise are in advanced energy management systems for future grids, the impact of large-scale integration of renewable energies on power system operations, stability monitoring and analysis of systems with high penetrations of renewables, and synchrophasor measurement applications on renewable integration.

Yong Liu (S'10-M'15) is currently a research assistant professor at the Department of Electrical Engineering and Computer Science at the University of Tennessee, Knoxville. He is also a member of the DOE/NSF-cofunded engineering research center CURENT. He received his B.S. and M.S. degree of Electrical Engineering from Shandong University in 2007 and 2010 respectively and obtained his Ph.D. degree from University of Tennessee, Knoxville, in 2013.

His research interests include power system wide-area measurement, renewable energy integration, and power system dynamic modeling and analysis.

Micah J. Till (S'13) received his B.S. in electrical engineering from Tennessee Technological University in 2011 and his M.S. in the same field from the University of Tennessee, Knoxville in 2015. He will be awarded his Ph.D. from the University of Tennessee in 2017.

His research interests include wide-area modeling, high-impact event scenarios, and phasor measurement unit applications.

Yilu Liu (F'04) received her M.S. and Ph.D. degrees from the Ohio State University, Columbus, in 1986 and 1989. She received the B.S. degree from Xian Jiaotong University, China.

Dr. Liu is currently the Governor's Chair at the University of Tennessee, Knoxville and Oak Ridge National Laboratory (ORNL). Dr. Liu is elected as the member of National Academy of Engineering in 2016. She is also the deputy Director of the DOE/NSF-cofunded engineering research center CURENT. Prior to joining UTK/ORNL, she was a Professor at Virginia Tech. She led the effort to create the North American power grid Frequency Monitoring Network (FNET) at Virginia Tech, which is now operated at UTK and ORNL as GridEye. Her current research interests include power system wide-area monitoring and control, large interconnection-level dynamic simulations, electromagnetic transient analysis, and power transformer modeling and diagnosis.